Supplementary information

Breakthrough in Large Area Photoanode Fabrication Process: High Concentration Precursor Solution with Solvent Mix and One Step Spin Coating for High PEC Performance of $BiVO_4$

Hoyoung Lee [a, b], Gil-Seong Kang [a], Hanyi Lim [a], Hyobin Han [b,c], Tae Woo Kim [c], Jun-Hyuk Choi [a], Dae-Geun Choi [a], Joo-Yun Jung [a], Jun-Ho Jeong [a], Jong Hyeok Park [b, *] and Jihye Lee [a, *]

[a] Nano Lithography and Manufacturing Research Center, Nano-Convergence Manufacturing Research Division, Korea Institute of Machinery & Materials (KIMM), 156 Gajeongbuk-ro, Yuseong-gu, Daejeon 34103, Republic of Korea

[b] Department of Chemical and Biomolecular Engineering, Yonsei University, 50 Yonsei-ro, Seodaemun-gu, Seoul 03722, Republic of Korea

[c] Hydrogen Research Department, Korea Institute of Energy Research (KIER), 152 Gajeong-ro, Yuseong-gu, Daejeon 34219, Republic of Korea

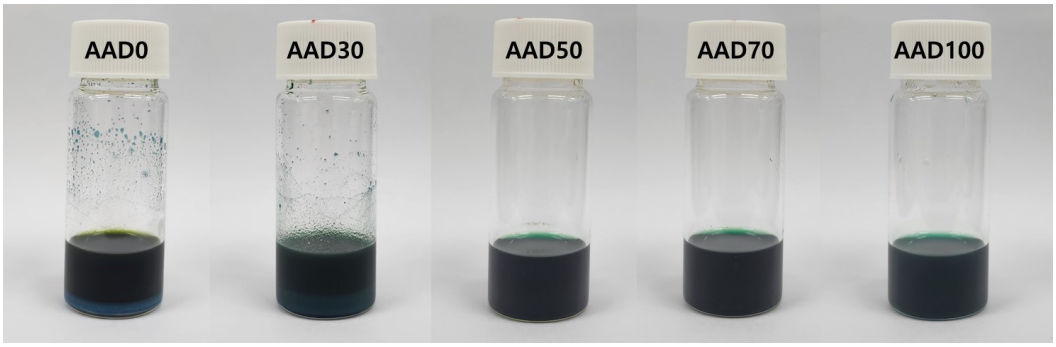

Fig. S1. The photograph of precursor solution with varying DMSO contents of 0, 30, 50, 70 and 100.

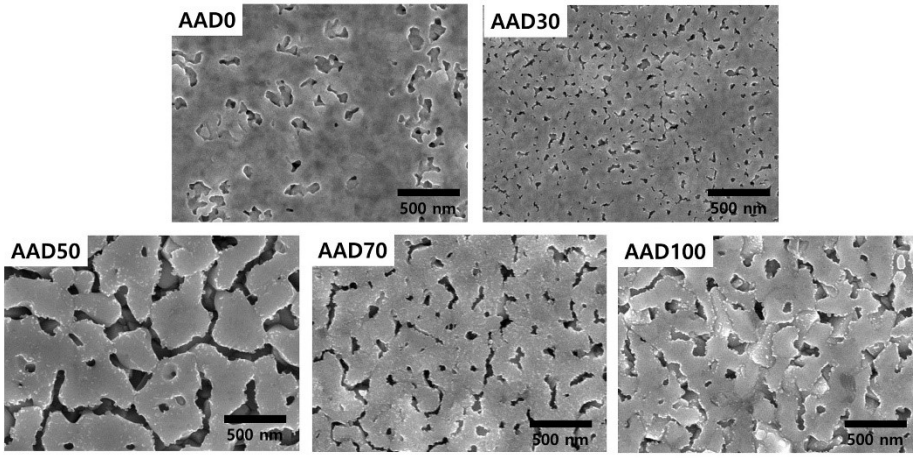

Fig. S2. Top view SEM images of BVO photoanodes by one-step spin coating with precursor solutions of varying DMSO contents of 0 (AAD0), 30 (AAD30), 50 (AAD50), 70 (AAD70) and 100 % (AAD100).

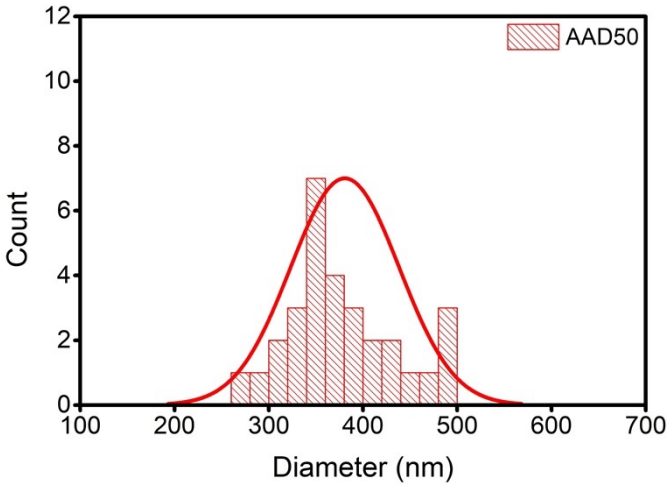

Fig. S3. Particle size (width) distribution curves obtained from the top-view SEM image of AAD50 BVO.

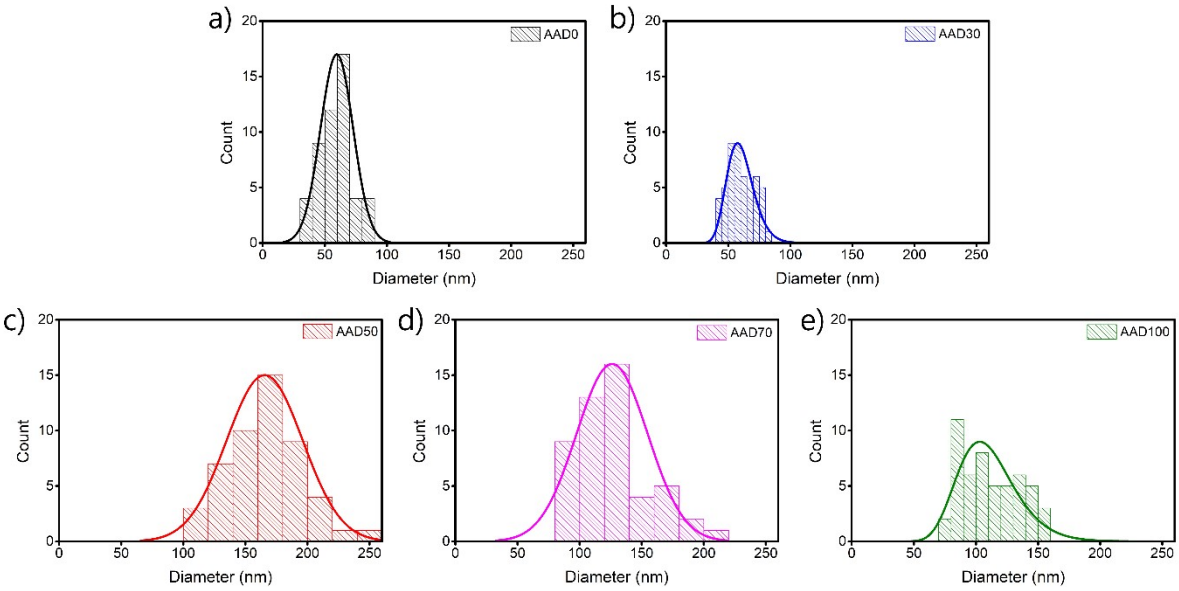

Fig. S4. Particle size (height) distribution curves obtained from the cross-sectional view SEM images of (a) AAD0, (b) AAD30, (c) AAD50, (d) AAD70, and (e) AAD100, respectively.

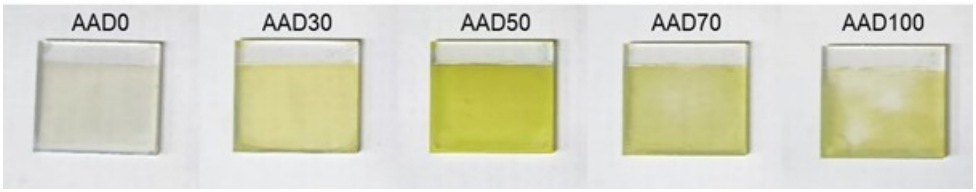

Fig. S5. Photo images of BVO photoanodes by one-step spin coating of different precursor solutions with varying DMSO contents of 0, 30, 50, 70 and 100% (AAD0, AAD30, AAD50, AAD70, AAD100).

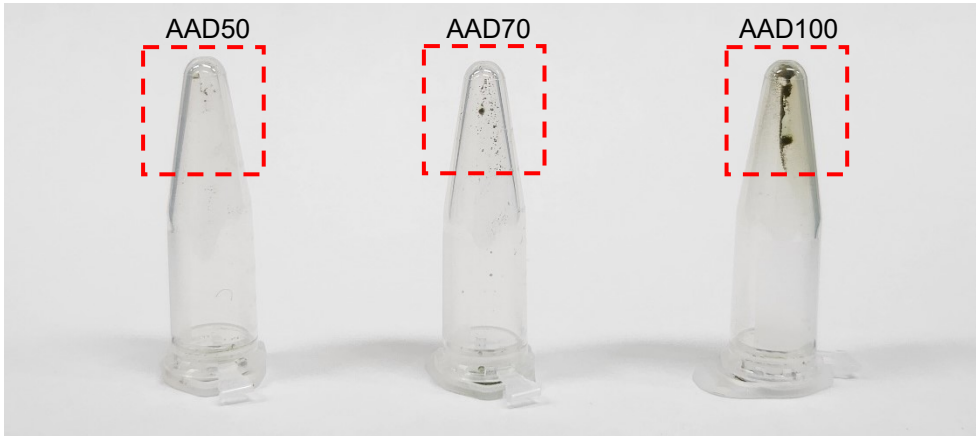

Fig. S6. Photo image of the precipitation of BVO precursor solutions with different DMSO contents of 50, 70 and 100% (AAD50, AAD70, AAD100) after aging for 1 day.

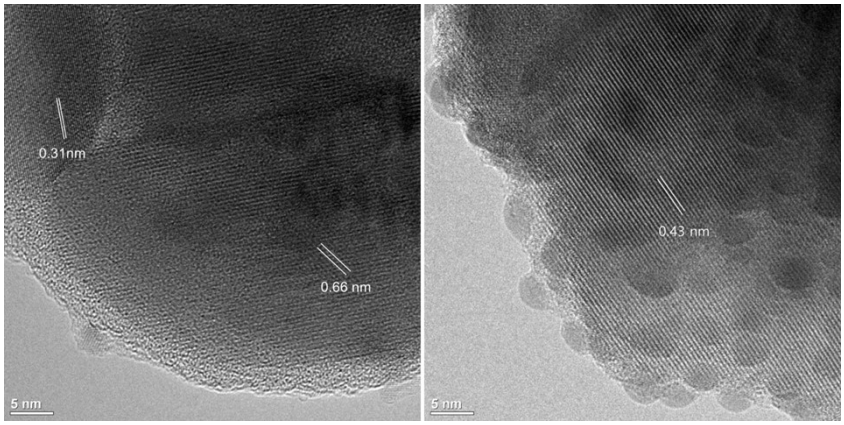

Fig.S7. HR-TEM images showing the lattice spacing of AAD 0 and AAAD 50.

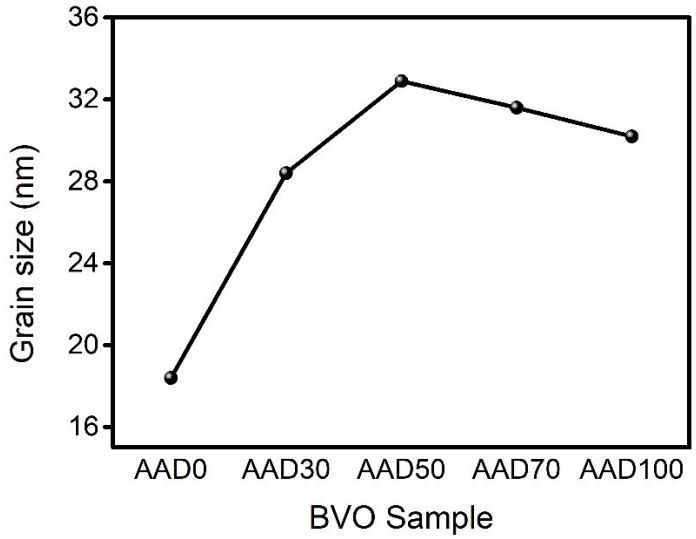

Fig. S8. Grain size of BVO film fabricated by using the different precursor solutions with varying DMSO contents.

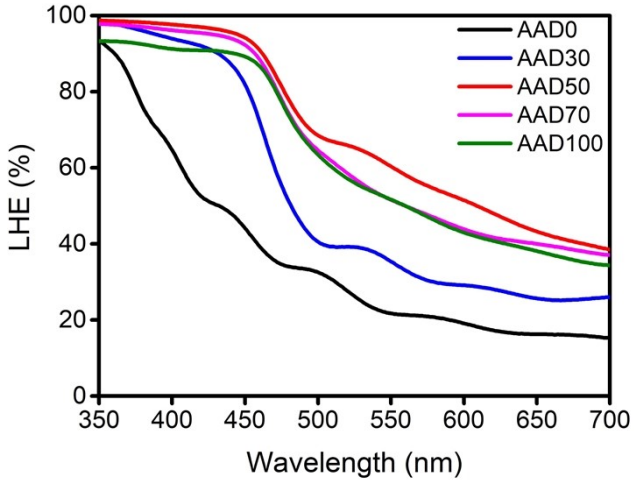

Fig. S9. Light harvesting efficiency (LHE) of the AAD0, AAD30, AAD50, AAD70, and AAD100 BVO at the incident wavelengths range from 350 nm to 700 nm.

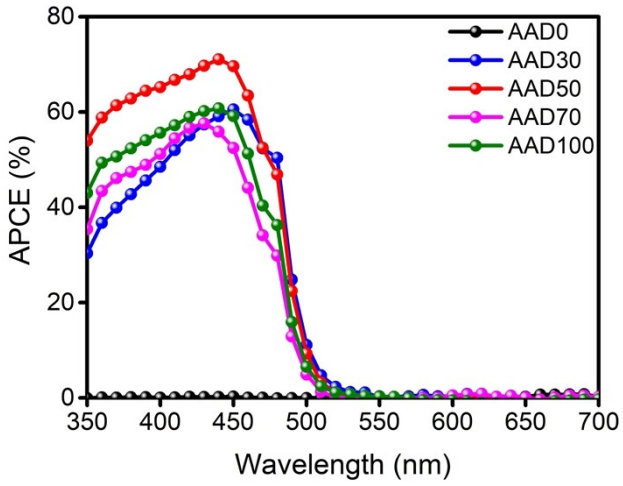

Fig. S10. Absorbed photon to current conversion efficiency (APCE) of the AAD0, AAD30, AAD50, AAD70, and AAD100 BVO at the incident wavelengths range from 350 nm to 700 nm.

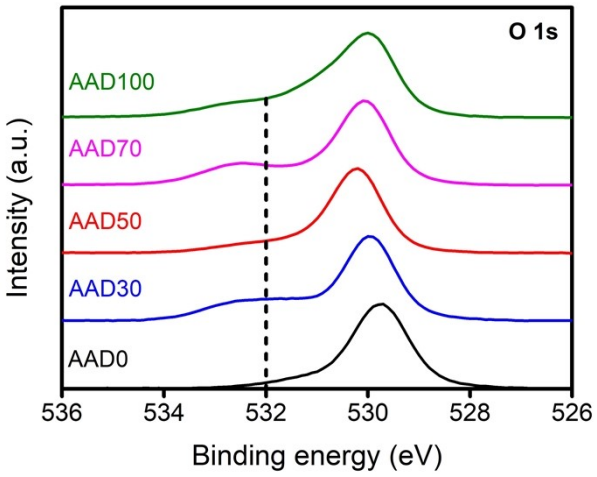

Fig. S11. X-ray Photoelectron spectroscopy (XPS) O1s spectra of AAD0, AAD30, AAD50, AAD70, and AAD100 BVO for intensity comparison at 532 eV.

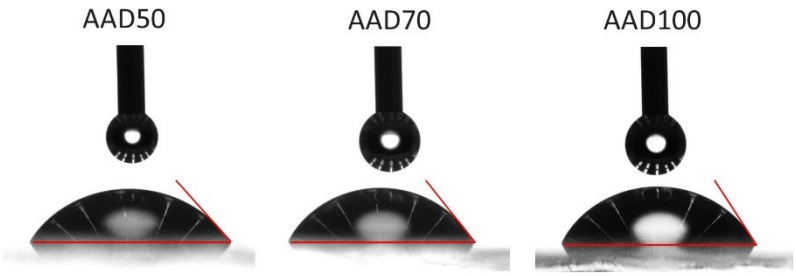

Fig. S12. The optical images of contact angle measurements for AAD50, AAD70, and AAD 100 BVO photoanodes with 10 µl of the PBS electrolyte**.** The measured contact angles for AAD50, AAD70, and AAD100 were 51.0, 55.2, and 62.1°, respectively.

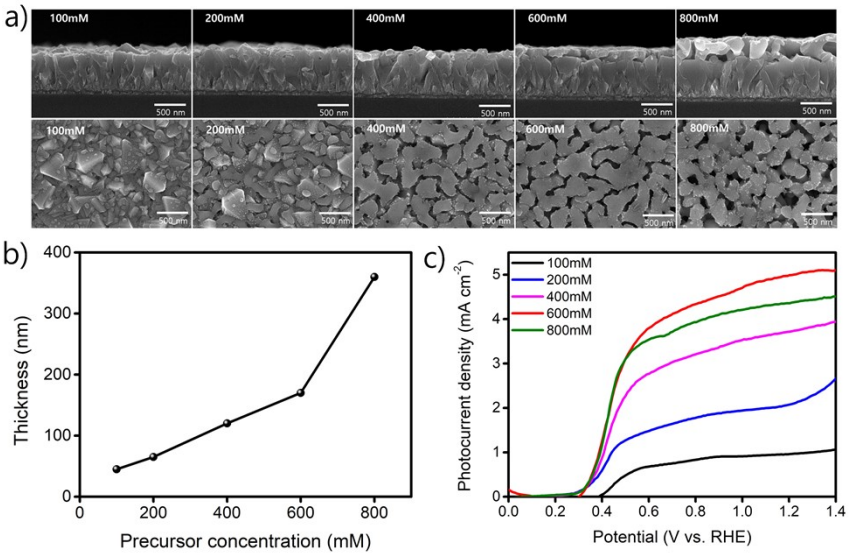

Fig. S13. (a) SEM images, (b) concentration vs. thickness graph and (c) LSV curves of BVO photoanodes from different precursor solutions with varying concentrations of 100, 200, 400, 600, and 800 mM (The Bi/V ratio was fixed at 0.9).

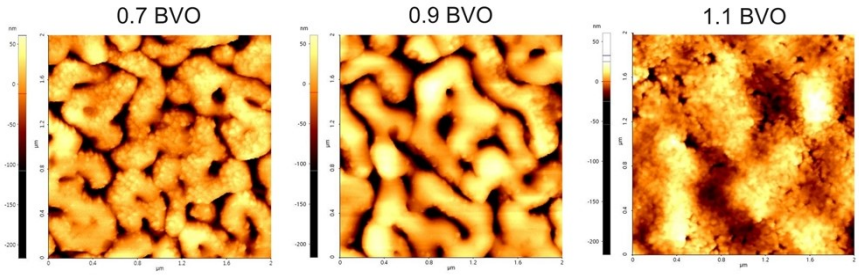

Fig. S14. Atomic force microscopy (AFM) images of 0.7 BVO, 0.9 BVO, and 1.1 BVO. The measured roughness for 0.7 BVO, 0.9 BVO and 1.1 BVO is 40.78, 49.95 and 9.21 nm, respectively.

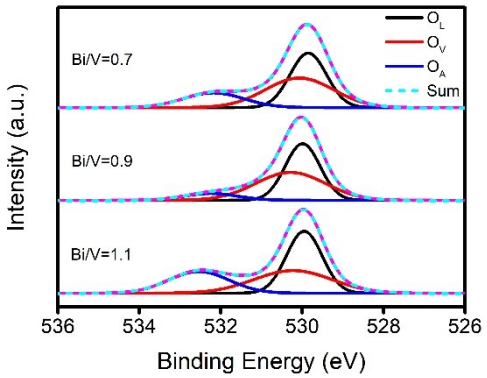

Fig. S15. XPS O1s spectra of BVO with Bi/V molar ratios at 0.7, 0.9, and 1.1, indicating deconvoluted components O_L, O_V, and O_A.

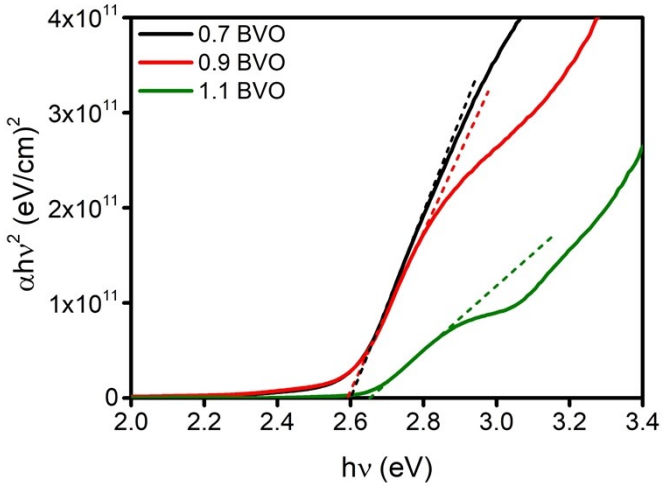

Fig. S16. Tauc plots for 0.7 BVO, 0.9 BVO and 1.1 BVO, derived from the optical absorbance data shown in Fig. 3d. In these plots, the point where the linear portion of the absorption edge intersects the horizontal axis indicates the optical bandgap of the semiconductor. The calculated optical bandgaps for 0.7 BVO, 0.9 BVO and 1.1 BVO are 2.60 eV, 2.59 eV and 2.66 eV, respectively.

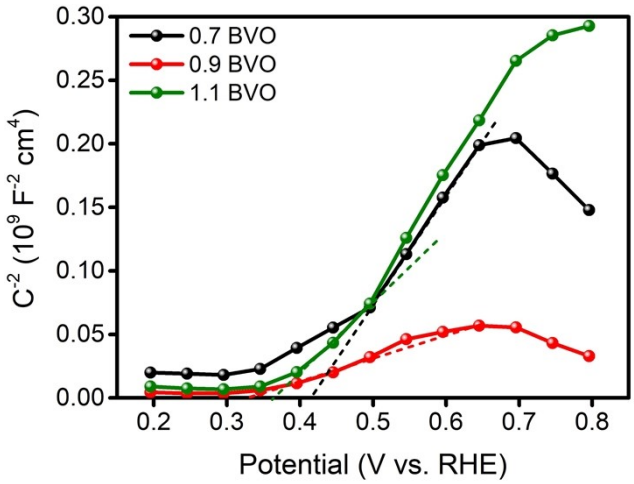

Fig. S17. Mott-Schottky (M-S) plot of 0.7 BVO, 0.9 BVO and 1.1 BVO. The calculated electron density for 0.7 BVO, 0.9 BVO and 1.1 BVO are 3.98, 10.9, and 3.53×10^{19} cm^{-3} respectively.

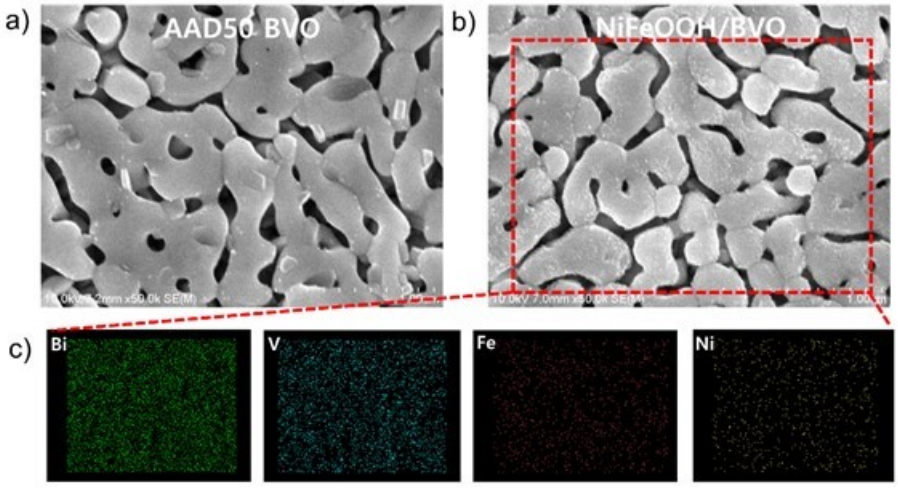

Fig. S18. Scanning Electron Microscopy (SEM) and Energy-Dispersive X-ray (EDX) Mapping Images of AAD50 BVO showing comparisons (a) before and (b-c) after photo-assisted electrodeposition of NiFeOOH.

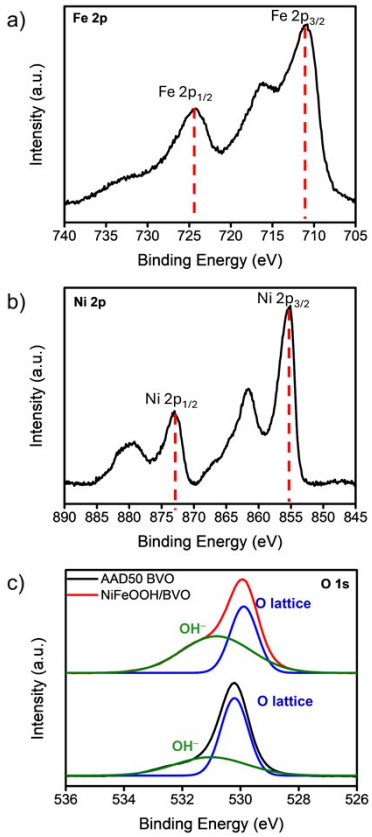

Fig. S19. XPS spectra of NiFeOOH/AAD50 BVO, (a) Fe 2p, (b) Ni 2p, and (c) O 1s. The Fe $2p_{3/2}$ (711.0 eV) and Fe $2p_{1/2}$ (724.5 eV) peaks and Ni $2p_{3/2}$ (855.5 eV) and Ni $2p_{1/2}$ (873.2 eV) peaks were clearly observed, indicating the presence of Fe^{3+} and Ni^{2+} states, respectively. In the O 1s spectrum, the two peaks observed at 531.6 eV and 529.5 eV correspond to the hydroxyl group (OH^-) and the oxide lattice (O^{2-}), respectively. A high ratio of OH^- to O^{2-} confirms the NiFeOOH/BVO.

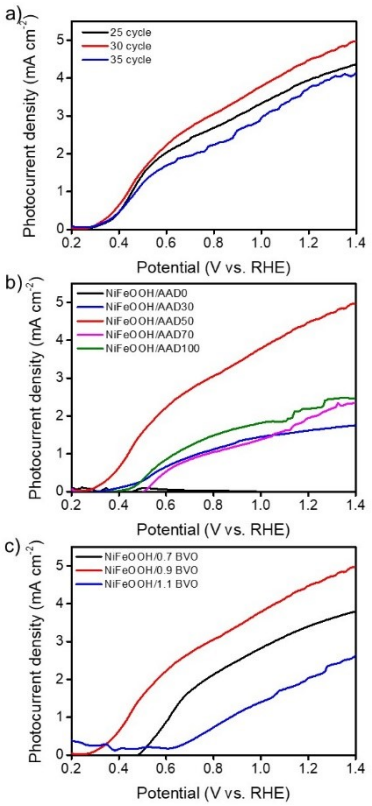

Fig. S20. Linear sweep voltammetry (LSV) curves of water oxidation in 0.5 M PBS electrolyte (a) for AAD50 BVO with NiFeOOH deposited in durations of 25 (black), 30 (red), and 35 (blue) cycles, (b) for BVO with different DMSO contents with NiFeOOH deposited in 30 cycles, (c) for BVO with different Bi/V molar ratios with NiFeOOH deposited in 30 cycles.

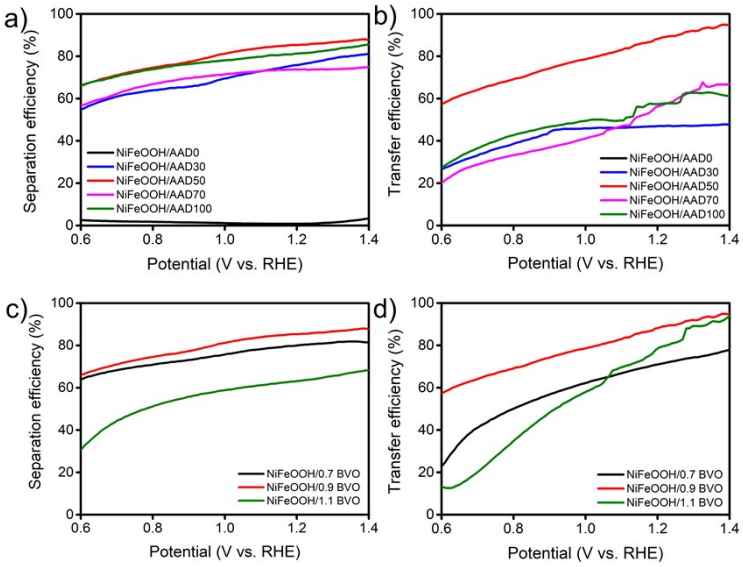

Fig. S21. (a) Charge separation and (b) transfer efficiencies of BVO photoanodes with varying DMSO solvent contents. (c) Charge separation and (d) transfer efficiencies of BVO photoanodes with different Bi/V molar ratios.

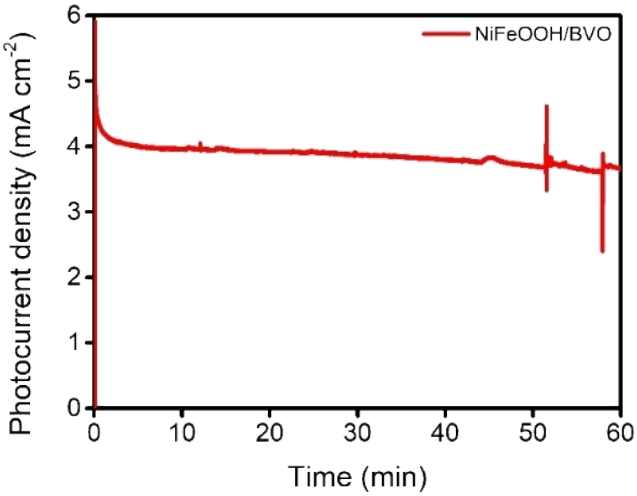

Fig. S22. The photocurrent of NiFeOOH/BVO over time during measurement of gas evolution at 0.5 M phosphate electrolyte at 1.23 V_{RHE} under AM 1.5G illumination.

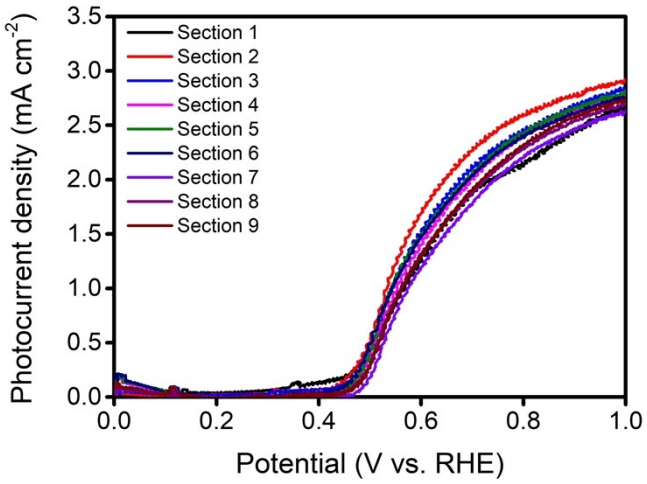

Fig. S23. LSV curves for the 144 cm² AAD50 BVO, measured at nine different points within a 9 cm² illumination area at 1.0 V_{RHE}. These results demonstrate the 144 cm² AAD50 BVO consistent photocurrent density across large areas.

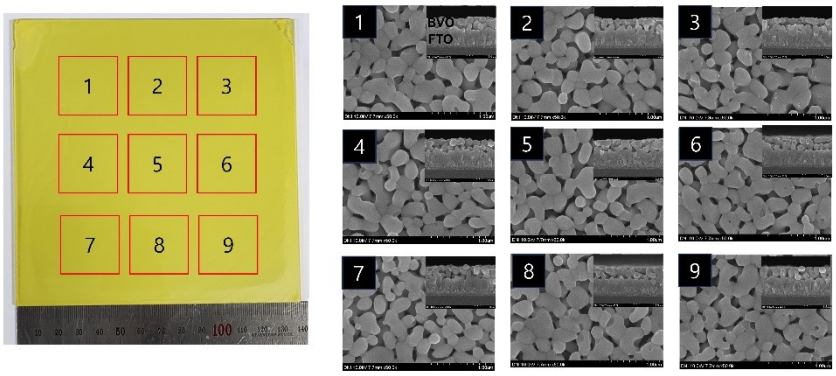

Fig. S24. Top view and cross-sectional images of the 144 cm² AAD50 BVO, corresponding to 9 distinct sections.

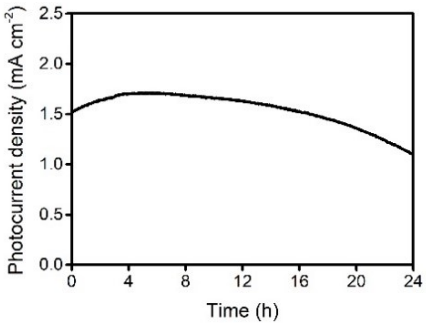

Fig. S25. The photocurrent stability of 144 cm^2 BVO photoanode at 0.5 M PBS electrolyte with 1.0 M Na_2SO_3 at 1.0 VRHE under AM 1.5G illumination.

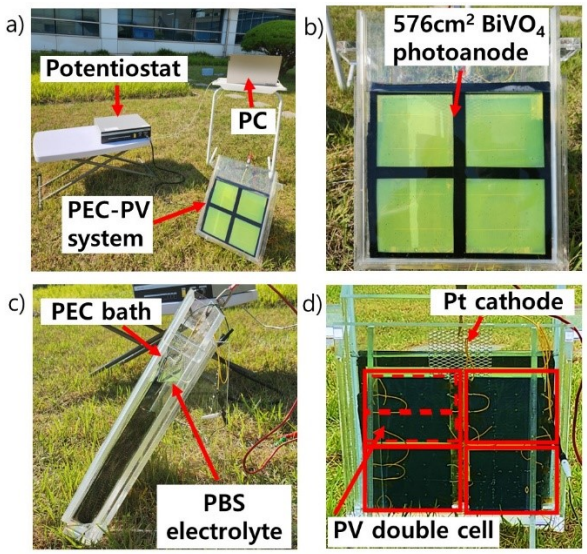

Fig. S26. Photoimages of PEC measurement setup of an ultra-large-scale self-driven PEC-PV system. (a) the entire measurement setup, and (b) the front view of PEC-PV system showing 576 cm2 BVO photoanode, (c) the side view showing PEC bath filled with PBS electrolyte, and (d) the rear view showing four PV double cells and Pt cathode.

Table S1. Comparison of XRD intensity of AAD0, AAD30, AAD50, AAD70, and AAD100 BVO with ratio of (040) to (121).

Samples	Intensity at 2θ values		Ratio of
	28.90 ° (121)	30.55 ° (040)	(040) to (121)
AAD0	37.08	5.97	0.16
AAD30	398.16	81.14	0.20
AAD50	344.02	191.74	0.54
AAD70	146.03	69.79	0.48
AAD100	204.76	50.99	0.24

Table S2. Fitted EIS results for AAD BVO photoanodes conducted in 0.5 M PBS containing 1.0 M Na_2SO_3 at 1.0 V_{RHE} under 1sun illumination.

Samples	R_s (Ω)	R_{ct} (Ω)
AAD0	25.76	609557
AAD30	27.79	7582
AAD50	26.37	4903
AAD70	32.69	6414
AAD100	20.69	6646

Table S3. Flat band potential and carrier density for AAD BVO photoanode using Mott-Schottky plots in 0.5M PBS with 1.0M Na_2SO_3 under dark conditions.

Samples	**Flat band potential V_{fb} (V_{RHE})**	**Carrier density N_d (10^{19} cm^{-3})**
AAD0	-0.180	1.3
AAD30	0.302	6.4
AAD50	0.307	10.9
AAD70	0.302	10.5
AAD100	0.275	4.7

Table S4. Nyquist plots from electrochemical impedance spectroscopy (EIS) data of the 0.7 BVO, 0.9 BVO, and 1.1 BVO obtained in phosphate electrolyte with Na_2SO_3 at 1.0 V vs. RHE under 1sun illumination.

Samples	**R_s (Ω)**	**R_{ct} (Ω)**
0.7 BVO	37.52	5283
0.9 BVO	26.37	4903
1.1 BVO	21.86	10500

Table S5. Flat band potential and carrier density for BVO photoanode related to Bi/V molar ratio using Mott-Schottky plots in 0.5M PBS with 1.0M Na_2SO_3 under dark Conditions.

Samples	Flat band potential V_{fb} (V_{RHE})	Carrier density N_d (10^{19} cm^{-3})
0.7 BVO	0.413	3.98
0.9 BVO	0.307	10.9
1.1 BVO	0.411	3.53